Integration of GNSS and Satellite InSAR Data: Derivation of Fine-Scale Vertical Surface Motion Maps of Po Plain, Northern Apennines, and Southern Alps, Italy

Gregorio Farolfi, Silvia Bianchini, and Nicola Casagli

Abstract—Global Navigation Satellite System (GNSS) and satellite synthetic aperture radar (SAR) interferometry represent the most important space geodetic techniques usually exploited to measure millimetric ground deformation on earth surface at both local and wide-area scale. SAR images processed with persistent scatterers interferometry (PSI) multitemporal approach lack of an absolute reference datum. In this paper, SAR images are calibrated with data derived from permanent GNSS stations, in order to obtain absolute and more accurate displacement values. The method used to correct PSI with GNSS is based on existing methodologies commonly applied in the geodetic practice of combining crustal and local deformation studies with geospatial statistical analysis. The spatial distribution of vertical terrain deformations and their temporal changes are coherently measured, leading to a fine-scale surface velocity map in the central-eastern Po Plain, Northern Apennines, and Southern Alps in Italy. The results reveal significant subsidence rates on the northwestern Adriatic coast including the Po Delta and the lagoon of Venice, as well as on Bologna and Ferrara cities in agreement with long-term displacement motion values provided by geological data and other previous works performed at local scale. This paper demonstrates the importance and effectiveness in creating a single, unique surface motion map by merging different data sets in which geodesy plays a relevant role in the datum alignment of PSI products before the stacking of the SAR maps.

Index Terms—Calibration, Global Navigation Satellite System (GNSS), integration, persistent scatterer interferometry (PSI), synthetic aperture radar (SAR).

I. INTRODUCTION

GLOBAL Navigation Satellite System (GNSS) and synthetic aperture radar (SAR) represent the most common space geodetic techniques used to study both local deformations and spatial and temporal changes in earth's lithosphere.

G. Farolfi is with the Italian Military Geographic Institute, 50121 Florence, Italy (e-mail: gregorio.farolfi@unifi.it).

S. Bianchini and N. Casagli are with the Department of Earth Sciences, University of Florence, 50121 Florence, Italy (e-mail: silvia.bianchini@unifi.it; nicola.casagli@unifi.it).

Color versions of one or more of the figures in this paper are available online at http://ieeexplore.ieee.org.

Researchers Bekaert *et al.* [1], Komac *et al.* [2], Simonetto *et al.* [3], and Catalão *et al.* [4] have long studied these methods and attempted to combine the two techniques; however, the problem is complex and spans several scientific disciplines, such as physics, geodynamics, estimation theory, differential geometry, and elasticity theory.

The first permanent GNSS networks were developed in the early 1990s; since then, a high number of networks have been distributed across many regions to collect high-quality data (with high signal-noise ratios, instrumentation, and antenna calibrations).

Persistent scatterers interferometry (PSI) is a technique applied to satellite SAR images that produce persistent scatterers (PS), which are sparse ground point-wise radar benchmarks characterized by long-term stability of the electromagnetic backscattered signal and high reflectivity [5].

These radar targets allow retrieving estimates of movement in terms of mean yearly velocity and single displacement measures at each acquisition date, along the satellite line of sight (LOS) with millimetric accuracy [6]. When a LOS diversity and much higher temporal sampling are needed for specific applications, ground-based SAR sensors can be used [7], [8].

The number of PS can change between different regions, depending on the number of available SAR images and on the presence of reflecting elements on the ground, both artificial (e.g., buildings, bridges, pylons, street lights, aboveground pipelines, and any rectilinear structure that can create a dihedral signal reflection back to the satellite) and natural (e.g., rocky outcrops, hard unvegetated surfaces, and boulders). Given that the PSI technique is based on a differential method, i.e., multitemporal interferometric approach, PS time-series analysis is a powerful technique for detecting and monitoring surface movements of unstable areas at a detailed scale (e.g., buildings and landslides). However, all the measurements are made in the satellite's LOS radar beam and are "relative" (not "absolute") measurements, both in space and time. This is because each measurement is referred temporally and spatially to, respectively, a unique reference image ("master" image) and to a stable point ("reference point") supposed to be motionless. The master scene is chosen in order to maximize the total coherence of the interferometric stack and to keep the

dispersion of the normal baseline values as low as possible. The selection of the reference point is arbitrarily made within a stable subarea of the investigated area of interest. Therefore, as PS are not georeferenced and their relative velocities must thus be corrected, the PSI technique is not an ideally stand-alone technique for studying larger areas involved in phenomena such as subsidence and uplift zones, but it requires comparison and calibration with other kind of information.

GNSS and PSI data sets are referenced to different reference systems. GNSS provides Cartesian geocentric data in the International Terrestrial Reference Frame 2008 (ITRF2008), which is updated from the ITRS89. GNSS velocity vectors can be transformed to the local system established on each site, where the vertical axis is the normal to the international ellipsoid (GR80), the horizontal plane is perpendicular to the normal, and north is orientated in the meridian direction passing through the site. The ground rates derived from PSI data are only estimated along the satellite LOS that is direction between the satellite sensor and the ground radar target.

These two techniques thus present complementary characteristics; GNSS data obtained from permanent stations are continuous, with high temporal resolution and low spatial resolution. PSI data yield a solution with low temporal resolution from the orbit-repeating cycle and a high number of point-wise benchmarks. The two techniques also differ somewhat in their sensitivities to the components of ground movements. In terms of vertical motion, SAR is more precise but less accurate than GNSS; with respect to horizontal motion, GNSS accurately measures both horizontal components, whereas SAR cannot detect movements along satellite ground track. SAR satellites with quasi-polar orbit and side-looking acquisition well detect movements along the east–west direction, while they provide less information about movements along the north–south direction. An additional drawback of the PSI technique is that it cannot recognize constant movements involving ground reference points, such as crustal movements that occur over large areas, and the accuracies of low wavenumber components of the velocity field decrease with increasing distance from them [9].

Thus, an important improvement in the combination of these techniques is a new, more detailed and coherent vertical velocity field, which is the topic of this paper.

Both techniques yield the velocities of a discrete number of ground points and sites, while the desired velocity field has a spatially continuous distribution. For this reason, both the method of interpolation and the geometrical approach play an important role in solving the problem.

The method used to validate PSI with GNSS is based on existing methodologies commonly applied in the geodetic practice of combining crustal and local deformation studies with geospatial statistical analysis.

II. AREA OF STUDY

In order to test the procedure, the southeastern Po Plain (Fig. 1), which is a wide foreland sedimentary basin bounded between the fold-thrust chains of Northern Apennines and Southern Alps [10], was chosen because it features a high rate of subsidence with strong spatial and temporal variations.
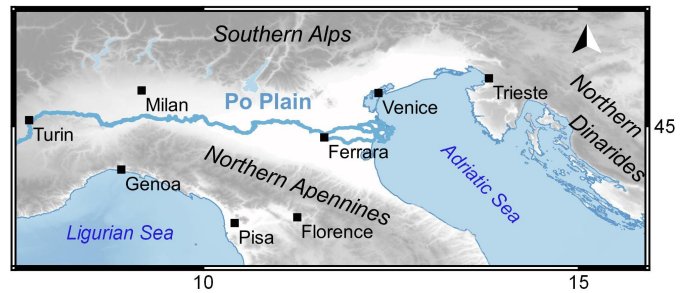

Fig. 1. Locations of the area of study including the southeastern Po Plain, a wide area of Italian peninsula between Northern Apennines and Southern Alps. Some important Italian cities are also pointed out.

The area of study presents one of the largest lowland of Europe that runs for 300 km along the north-western Adriatic coast including the Po Delta and the lagoon of Venice. It includes lagoons, distributary bays, salt and fresh-water wetlands, channels system, and rivers that flow from the Alps and Apennines. Thus, this area stands out for nature and also culture, as important UNESCO heritages such as Venice, Ravenna, and Ferrara rise up.

This area has a dense distribution of PSI data and 177 permanent GNSS stations that allow the process of validating the time series and calculating vertical velocities.

The validation process is based on the comparison of GNSS and SAR data sets, using their complementary features to check and then correct each single technique before merging all the data. The high spatial distribution of information in the area of study provides a more detailed field of study of the subsidence and also provides a better understanding of the processes of deformation.

The subsidence of the selected study area is twofold: first, it is partly due to anthropogenic causes, driven by water and gas exploitations during last century; second, it is also due to tectonic processes, including the subsidence of Po Plain and the northern Adriatic Sea and the uplifting of the nearby Alps, Apennines, and Dinarides [11]–[17].

III. DATA SETS AND TECHNIQUES

The ideal condition for the comparison between two different time series is to have both measurements performed both at the same site and in the same period of time. SAR ENVISAT frames in ascending and descending geometries cover the whole area where GNSS stations are located (Fig. 2), and the SAR processing output is discrete point-like PS benchmarks. As the spatial problem of correlation of the two kinds of data can be solved through interpolation, the temporal condition was corrected by noting that the GNSS and PSI data sets overlap for more than eight years and by using the hypothesis of linear motions. The PSI product is obtained by sampling and cropping different original SAR frames and tracks. Because each frame has its own reference, arbitrarily selected by the firm who processed the original images, therefore at least one GNSS station is necessary to shift all the cluster to the same common reference.

A. GNSS

The GNSS velocity field of the southeastern Po Plain has been derived by the combination of two independent
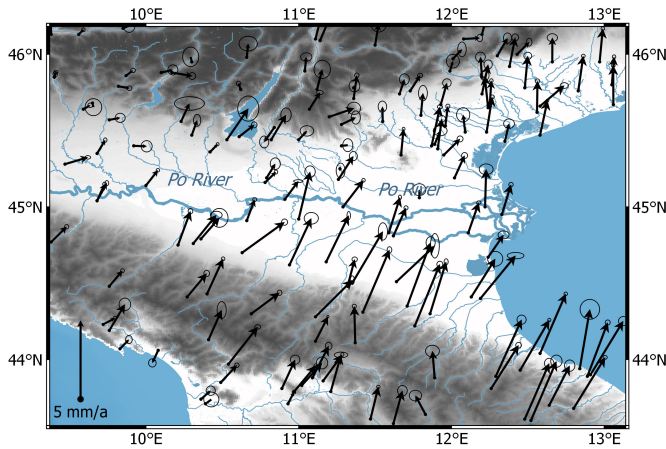
Fig. 2. Horizontal velocities of GNSS permanent stations over the study area and their ellipses of error (95% confidence level) represented in the European reference system (ETRS89). Background is shaded-relief map ETOPO1 Global Relief Model Topography [30].
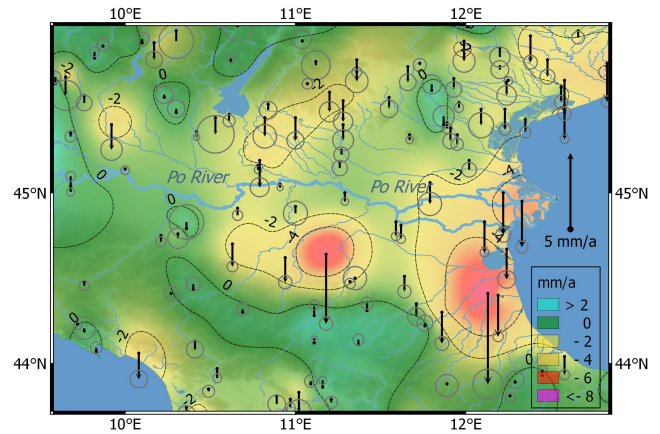

Fig. 3. Vertical velocities bars and errors circles with 95% confidence level calculated from GNSS permanent stations displayed over the study area. Background vertical velocity field contour plot are determined with multilevel B-spline interpolation model [31]. Green represents the stable area, cyan represents areas with uplift ≥2.0 mm/a, and orange represents areas with subsidence ≤−2.0 mm/a.

solutions consists of a subset of 177 sites extrapolated from the computation of 784 permanent GNSS stations displaced in the Italian Peninsula and surround it.

Both velocity solutions were determined by using a new absolute antenna phase center correction model (igs08), through precise orbits recomputed in 2014 by the International GNSS Service (IGS), following the International Earth Rotation and Reference Systems Service Conventions 2010 [18], the EUREF guideline 2013 [19], and a new function to calculate the tropospheric delay [20]. Single weekly normal equations, aligned to ITRF2008, were analyzed to determine the linear velocity by checking for possible outliers and estimating the periodic annual and semiannual fluctuations.

The first velocity solution is the result of the processing of 113 permanent GNSS stations that belong to the Italian GNSS geodetic network [21] calculated for a time period of 6.5 years [22], [23]. Data processing was carried out using Bernese GPS Software [24] and velocity errors were estimated using the maximum-likelihood estimation technique (CAT Software) [25], which modeled the correlated noise with a combination of flicker and white noise.

The second velocity solution [26] was obtained by using the GAMIT/GLOBK software packages [27]. This data set consists of 784 continuous GNSS stations with more than 2.5 years of observations. The velocity uncertainties were estimated adopting the first-order Gauss–Markov extrapolation algorithm proposed by Herring [28].

The two velocity solutions were compared by treating the velocity differences as a stochastic process. A time-derivative Helmert transformation involving a rigid roto-translation (six parameters) were applied to minimize the differences of the two velocity frames by using a least-squares approach. Then, a weighted combination provided the final velocity solution.

The horizontal ITRF2008 velocities were transformed into the European Terrestrial Reference Frame ETRF2008 (Fig. 2) by applying a rigid roto-translation [29]; vertical velocities of GNSS data in the period 2008–2014 over the Po plain

obtained through surface interpolation are drawn in Fig. 3, where stability range was set within ±2 mm/a and displayed in green, while cyan and orange colors, respectively, represent areas with ground uplift ≥2.0 mm/a (millimeter per annum) and ground lowering ≤−2.0 mm/a.

B. SAR

The ground surface deformation measurements were calculated by PSI processing with PSInSAR approach [5] using all available ENVISAT data from the Italian peninsula. These SAR displacement measurements are a part of the program "not-ordinary plan of remote sensing" developed by the Italian Ministry of the Environment with the purpose of mapping to prevent geohazards and available from the Italian Geoportale Nazionale (www.pcn.minambiente.it).

The ENVISAT mission presents a temporal solution of 35 days (which represents the satellite's repeat cycle) and covered a long-term continuous period from 2003 to 2010. The ENVISAT program was a continuation of the European remote sensing (ERS) 1 and 2 missions, which provided long-term continuous data from 1992 to 2000 and were primarily intended for scientific research.

Ground movements were measured along the LOS with an offnadir angle of 23° (angle defined by the incident radar beam and the vertical to the ground) on a grid of point-like benchmarks on the ground. A negative sign of the movement stands for an increasing distance of the benchmark from the satellite sensor, while a positive sign means a movement toward the satellite. Within the PSI velocity, for distinguishing stable targets (displayed in a green color) from moving ones, stability threshold is fixed at ±2 mm/a for all the data frames, according to the standard deviation value of the PSI populations and to minimum value exceeding the precision of the PSI technique. These values are also in accordance with stable threshold choices already tested and accepted by the scientific community [32]–[36]. In the study area, the spatial distribution of LOS mean yearly velocities recorded by ENVISAT satellite in the time span 2003–2010 in ascending
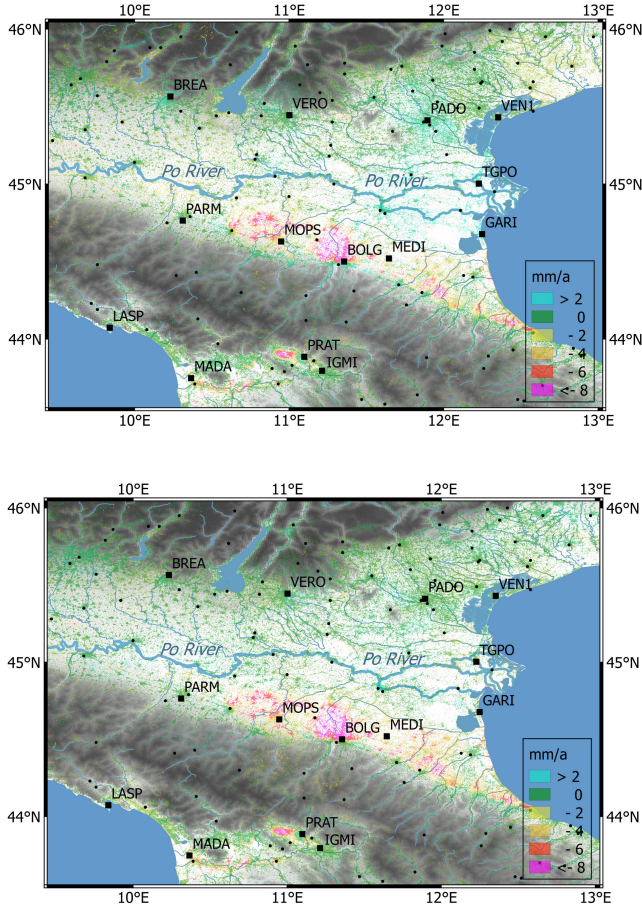
Fig. 4.   Velocity maps of PSI ENVISAT points, GNSS permanent station sites (black points), and some selected of them (black squares). (Top) Ascending LOS velocities. (Bottom) Descending LOS velocities.
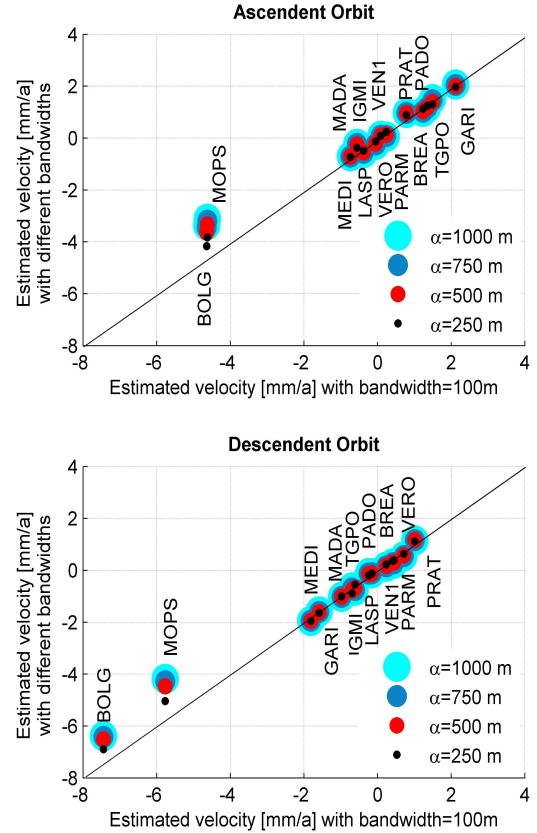

Fig. 5.   Comparison of PSI LOS velocities determined in the area around a subset of 14 GNSS locations with different inverse exponential weighting bandwidths for (Top) ascending and (Bottom) descending orbits. Five series of calculated PSI LOS velocities with different bandwidths (250, 550, 750, and 1000, see legends) are compared with those with a bandwidth of 100 m. Black lines represent the isolines of the 100 m bandwidths; discrepancies are shown as increasing distance of points from the isoline.

and descending orbits provide similar values in both sign and intensity, demonstrating almost vertical ground movements.

LOS mean yearly velocities of PSI ENVISAT data (Fig. 4) show an overall stability north of the Po River on the Southern Alps belt, while the southern portion of Po Plain toward Northern Apennines reveal diffuse subsiding areas nearby Modena and Bologna cities and Adriatic coastline (around Ravenna and Rimini cities), with estimated average deformation rates lower than −2 mm/a. Some areas with downward motion of surface can be also recognized south of Northern Apennines chain, i.e., north-west of Prato (PRAT) city and between Pisa city (Madonna Dell'Acqua site) and Florence city (Italian Military Geographic Institute site).

IV. PSI OUTCOME CALIBRATION

A. Stability of GNSS Sites

To compare the two data sets, the PS velocities of ascending and descending orbits must be calculated for each GNSS site. Since it is rare for a PS point to be located in the same position as a GNSS station, an interpolation procedure should be applied.

PS velocities for ascending and descending orbits are calculated by interpolation, using a cloud of PS around each GNSS sites to apply a deterministic method with inverse

distance weighting [37], [38]. The interpolated value v at a given point $\mathbf{p} = (\mathbf{x}, \mathbf{y}, \mathbf{z})$ based on samples $v_i = v(\mathbf{p_i})$ located at position $\mathbf{p_i} = (x_i, y_i, z_i)$ for $i = 1, 2, \ldots, N$ is given by

$$v(\mathbf{p}) = \frac{\sum_{i=1}^{N} w_i(\mathbf{p}) v_i}{\sum_{i=1}^{N} w_i(\mathbf{p})} \tag{1}$$

where the weight $w_i(\mathbf{p})$ is the negative exponential function of its Euclidean distance $d(\mathbf{p}, \mathbf{p_i},)$ from $\mathbf{p_i}$ to $\mathbf{p}$

$$w_i(\mathbf{p}) = \exp\left(-\frac{d(\mathbf{p}, \mathbf{p_i},)}{\alpha}\right) \tag{2}$$

where α is the bandwidth.

The choice of the bandwidth is important because it produces different results: short bandwidths give a higher weight to closer points than to ones that are farther away. In this paper, the interpolation of PS velocities was carried out using different bandwidths (Fig. 5) because discrepancies yield information about the stability of the GNSS site, which is usually a building.

These discrepancies thus typically register the presence of a local movement; therefore, GNSS sites should not be used to account for geodetic and geodynamic scopes.

B. Determination of PSI Velocity Maps

The LOS direction of satellite SAR is referenced to the vertical direction, normal to the equipotential surface of gravity from the SAR satellite. In contrast, GNSSs represent local velocities with respect to the normal of the ellipsoid of points at each station. These data sets can be directly compared, assuming that the difference between the vertical of the SAR satellite and the normal of an ellipsoid is negligible. The velocity v_{LOS} measured by the SAR satellite can thus be represented by the unit vector S, which travels from the ground to the satellite (LOS direction) and is defined as

$$v_{\text{LOS}} = v_{\text{North}} S_{\text{North}} + v_{\text{East}} S_{\text{East}} + v_{\text{Vert}} S_{\text{Vert}} \qquad (3)$$

and the velocities measured by the SAR satellite in ascending and descending orbits can be written as

$$\begin{pmatrix} v_{\text{Asc}} \\ v_{\text{Des}} \end{pmatrix} = \begin{pmatrix} S_{\text{North,Asc}} & S_{\text{East,Asc}} & S_{\text{Vert,Asc}} \\ S_{\text{North,Des}} & S_{\text{East,Des}} & S_{\text{Vert,Des}} \end{pmatrix} \begin{pmatrix} v_{\text{North}} \\ v_{\text{East}} \\ v_{\text{Vert}} \end{pmatrix}. \qquad (4)$$

Equation (4) can be written as a function of the inclination of the orbits with respect to the equator, ζ, and the mean offnadir, ε

$$\begin{pmatrix} v_{\text{Asc}} \\ v_{\text{Des}} \end{pmatrix} = \begin{pmatrix} -\sin\varepsilon\cos\zeta & -\sin\varepsilon\sin\zeta & \cos\varepsilon \\ \sin\varepsilon\cos\zeta & \sin\varepsilon\sin\zeta & \cos\varepsilon \end{pmatrix} \begin{pmatrix} v_{\text{North}} \\ v_{\text{East}} \\ v_{\text{Vert}} \end{pmatrix}. \qquad (5)$$

For ENVISAT satellites, in which the inclination of the orbits with respect to the equator is 98.5° and the mean offnadir is 23°, the modules of components of S are [0.05, 0.38, 0.92].

Equation (5) is a system of two equations with three variables and is thus not solvable. Displacements occurring along the north–south direction, almost parallel to the satellite orbit, cannot be measured accurately, as their projection along the LOS is negligible for both ascending and descending orbits. Assuming that the projection of the north component of velocity along the LOS is negligible, (5) can be approximated as

$$\begin{pmatrix} v_{\text{Asc}} \\ v_{\text{Des}} \end{pmatrix} \cong \begin{pmatrix} -\sin\varepsilon & \cos\varepsilon \\ \sin\varepsilon & \cos\varepsilon \end{pmatrix} \begin{pmatrix} v_{\text{East}} \\ v_{\text{Vert}} \end{pmatrix}. \qquad (6)$$

The vertical velocity v_{Vert} and the east component of velocity v_{East} can be calculated as

$$\begin{pmatrix} v_{\text{East}} \\ v_{\text{Vert}} \end{pmatrix} \cong \frac{1}{2\sin\varepsilon\cos\varepsilon} \begin{pmatrix} -\cos\varepsilon & \cos\varepsilon \\ \sin\varepsilon & \sin\varepsilon \end{pmatrix} \begin{pmatrix} v_{\text{Asc}} \\ v_{\text{Des}} \end{pmatrix}. \qquad (7)$$

Now, the velocity v_{LOS} is approximated to the 2-D unit vector T pointing from the ground to the satellite

$$v_{\text{LOS}} \cong v_{\text{East}} T_{\text{East}} + v_{\text{Vert}} T_{\text{Vert}} \qquad (8)$$

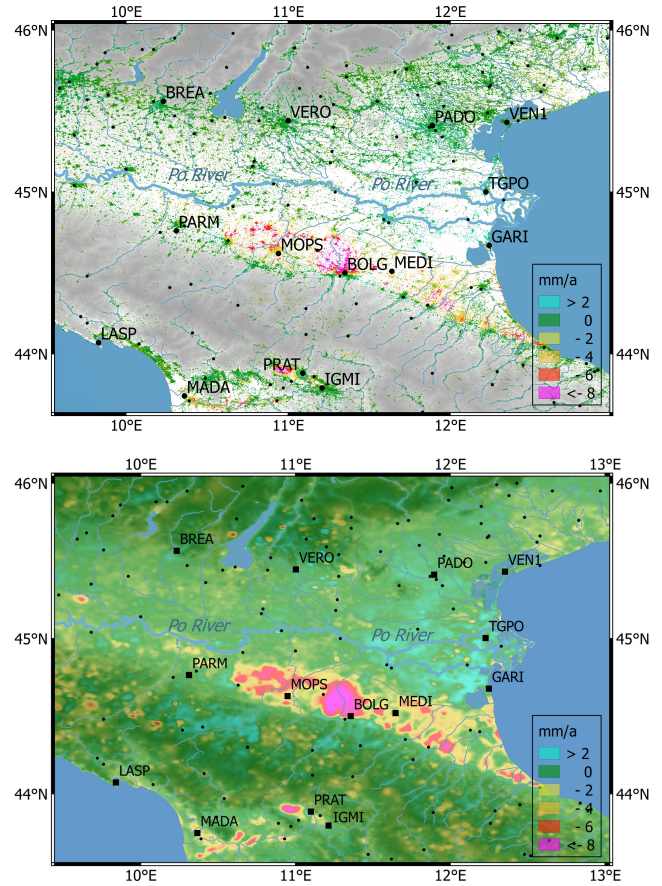where T has the components [0.39, 0.92] for ENVISAT satellites.

Fig. 6. (Top) Vertical velocities of PSI points determined by combination of ascending and descending LOS velocities calculated for the cells that present both values. (Bottom) Vertical velocities map derived by multilevel B-spline interpolation [31] of sparse PSI points calculated for a regular grid with cells of 0.25 km × 0.25 km. Green represents the stable area, cyan represents areas with uplift of 2.0 mm/a, orange–pink represent areas with downward movement of less than −4 mm/a, and violet represents areas of downward movement less than −8.0 mm/a.

C. Comparison of Vertical Velocities Derived by SAR and GNSS

The vertical velocity map derived by the combination of the velocities measured by the SAR satellite in ascending and descending orbits (7) is represented in Fig. 6.

Comparison of vertical velocities calculated using SAR and GNSS are shown on map of Fig. 7. PSI velocities were calculated using a cloud of PS around each GNSS site and merged by applying a distance scaling function $w(d) = \exp(-d/\alpha)$ with $\alpha = 100$ m.

In particular, north of the Po Delta, the historical town of Venice, which lies into a barrier island lagoon system swamped by high tides and floods, appears to be stable and no longer affected by subsidence, as also stated by some recent works [11], [15], [39] (Fig. 8, top left).

In the alluvial plain, maximum subsidence rates up to 26–28 mm/a, occur in the urban zone of Bologna with an increasing spatial pattern northwards (Fig. 8, top right). Present intense subsidence in this area started during the second half of the 20th century, due to sharp increase of groundwater withdrawal following an accelerating economic growth [11]. The area around Modena city also experiences strong terrain

TABLE I

COMPARISON OF GNSS AND SAR VELOCITIES AND COMPONENTS (VERTICAL AND EAST) AND
THEIR ERRORS DISPLAYED FOR SOME REPRESENTATIVE GNSS PERMANENT SITES

| STAT	LON	LAT	GNSS velocity (mm/a)			GNSS velocity errors (mm/a)			SAR velocity (mm/a)		SAR velocity error (mm/a)		Velocity comparison GNSS-SAR (mm/a)	
			N	E	U	N	E	U	U	E	U	E	U	E
BOLG	11,35	44,50	3,3	2,0	0,0	0,3	0,6	1,3	-6,5	-3,6	0,7	1,7	6,5	5,6
BREA	10,23	45,56	1,2	0,6	-0,1	1,0	0,5	1,0	0,9	-1,3	0,5	1,2	-1,0	1,9
GARI	12,24	44,67	1,5	1,0	-3,3	0,4	0,3	1,0	0,3	-4,8	0,4	0,8	-3,6	5,8
IGMI	11,21	43,79	2,4	0,7	-0,3	0,5	0,2	0,7	-0,5	-0,3	0,3	0,7	0,2	1
LASP	9,83	44,07	0,6	0,6	0,4	0,3	0,3	0,7	-0,2	0,2	0,5	1,1	0,6	0,4
MADA	10,36	43,74	0,6	0,7	-0,8	0,3	0,4	1,1	-0,9	-0,4	0,4	0,9	0,1	1,1
MEDI	11,64	44,51	2,3	2,5	-1,6	0,3	0,8	0,8	-1,2	-1,7	0,4	0,8	-0,4	4,2
MOPS	10,94	44,62	3,0	1,4	-0,6	0,5	0,4	0,8	-5,6	-1,5	0,5	1,1	5,0	2,9
PADO	11,89	45,41	0,9	0,4	-0,6	0,5	0,4	0,6	0,7	-2,1	0,5	1,2	-1,3	2,5
PARM	10,31	44,76	1,9	1,5	2,4	0,4	0,3	1,2	0,4	0,2	0,5	1,0	2,0	1,3
PRAT	11,09	43,88	2,1	1,1	0,9	0,3	0,3	0,7	1,0	0,2	0,3	0,7	-0,1	0,9
ROVE	11,04	45,89	0,9	0,1	0,2	0,4	0,3	1,1	0,0	1,2	0,7	1,5	0,2	-1,1
TGPO	12,22	45,00	2,4	0,1	-4,6	0,5	0,4	0,9	0,5	-2,9	0,4	0,9	-5,1	3
VEN1	12,35	45,43	1,2	0,3	-1,4	0,4	0,4	0,7	0,2	0,5	0,4	0,9	-1,6	-0,2
VERO	11,00	45,44	0,6	0,6	-2,4	0,5	0,4	1,0	0,5	0,8	0,6	1,3	-2,9	-0,2
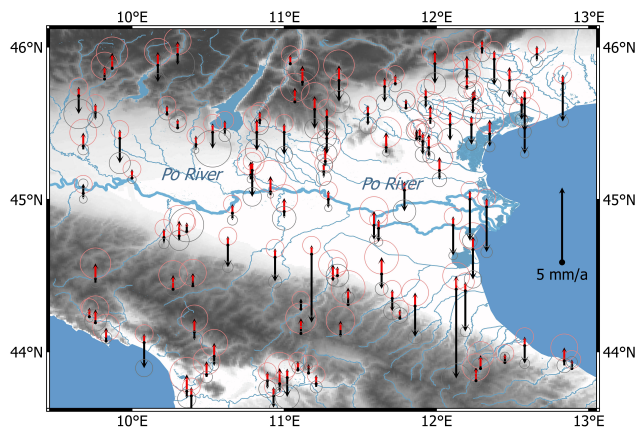
Fig. 7. Map of vertical velocities and errors circles with 95% confidence level determined by GNSS (black) and PSI (red) techniques for each GNSS permanent sites. Red arrows represent the vertical velocities calculated with PS points displaced approximately 100 m from each GNSS permanent site. Black arrows represent the vertical velocities calculated by GNSS processing. Some results are displayed on Table I.

subsidence with velocity values up to 19 mm/a in the satellite monitoring period 2003–2009 (Fig. 8, bottom left). These values are consistent with subsidence rates recorded by means of SAR interferometry by [16] and [40].

South of Northern Apennines fold-thrust belt, the Florence–Prato–Pistoia area is also affected by high rates of vertical ground movements. On one hand, the city of Prato is characterized by a terrain uplift, with rates of about 5 mm/a, related to the drastic reduction of the water extraction determined by crisis of the textile industrial district in the observation period; on the other hand some areas are subsiding NW of Prato, nearby Pistoia city, reaching average vertical velocity values of 20–25 mm/a, due to the water exploitation for extensive plant nursey districts in this area (Fig. 8, bottom right).

Full time series of vertical displacement of some significant PS benchmarks collected for the whole period of SAR monitoring (2003–2009) are reported in Fig. 9 as well as temporal series of GNSS stations. For each site, the PS radar target as the most representative and nearest to the GNSS station was chosen to be shown in the graphs of Fig. 9. The graphs show an overall stability on the Venice site (VEN1), while Bologna (BOLG) and Modena (MOPS) sites are dominated by downward vertical motion with a linear and almost constant pattern across time. The PRAT site on Prato city reveals an uncorrelated trend that means general stability, as displacement that varies randomly over time, and possibly a slight uplift, since the GNSS site is located on a stable area out of the moving zones, as shown in Fig. 8.
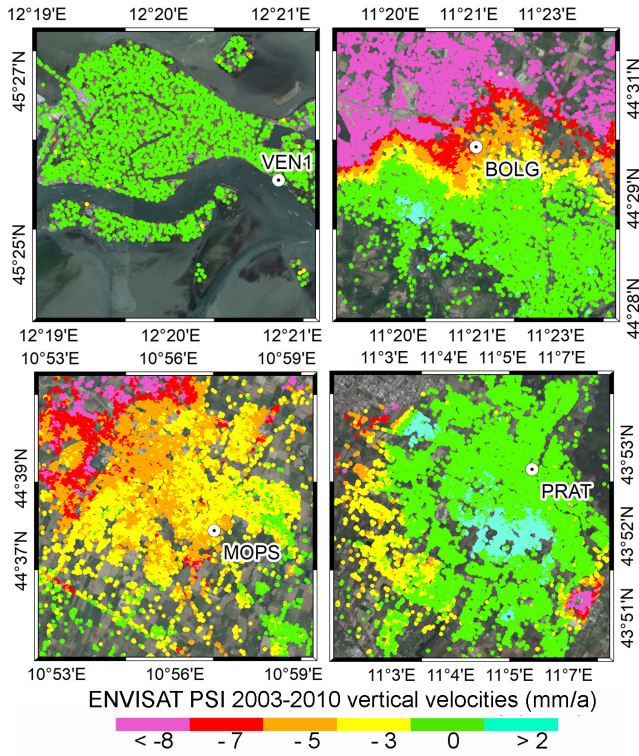
Fig. 8. Vertical velocity maps of PSI ENVISAT data. GNSS permanent station is shown with white points. Background layers are digital color aerial orthophotos "Volo Italia" acquired in 2000, with 1 m resolution. (Top Left) Venice (VEN1) site. (Top Right) Bologna (BOLG) site. (Bottom Left) Modena (MOPS) site. (Bottom Right) Prato (PRAT) site.
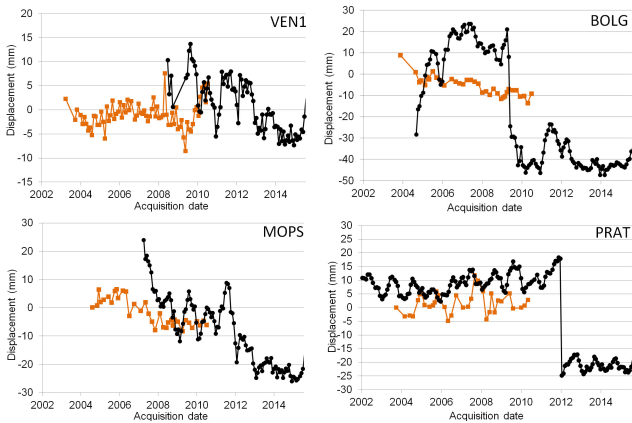

Fig. 9. Vertical displacement time series of representative PS benchmarks compared to vertical displacement of four GNSS stations. (Top Left) Venice (VEN1) site. (Top Right) Bologna (BOLG) site. (Bottom Left Modena (MOPS) site. (Bottom Right) Prato (PRAT) site. BOLG site presents a discontinuity at Julian day 137 of the year 2009 but any information is related to this event, while the discontinuity of PRAT (340/2011) is due to the change of antenna and receiver. In any case, the linear velocity of each GNSS site is calculated after the determination of discontinuities and the estimation of annual and semiannual seasonal fluctuations.

D. Calibration and Data Integration

The offset calibration $v_{\mathrm{PSIOC},i}$ of PSI data set was performed for each i-GNSS permanent site as the difference of vertical velocities determined by the two techniques

$$v_{\mathrm{PSIOC},i} = v_{\mathrm{GNSS},i} - v_{\mathrm{PSI},i} \quad \text{for each } i\text{-GNSS site} \quad (9)$$
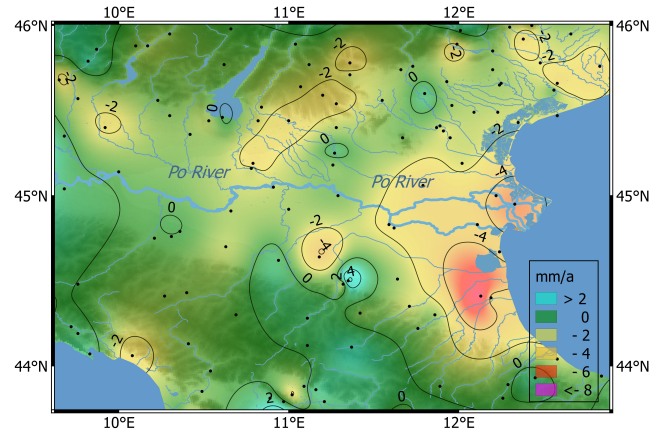

Fig. 10. Vertical velocity corrections contour plot to apply to original PSI data set. Green represents the area where no correction is due. Cyan represents areas where the correction of vertical velocity is positive ≥ 2.0 mm/a. Yellow–orange represents areas where the correction of vertical velocity is negative ≤ -2.0 mm/a.

then, sparse points $v_{\mathrm{PSIOC},i}$ were interpolated with multilevel B-spline model [31] to create a smooth surface of vertical correction $v_{PSICorr}$ (Fig. 10). Multilevel B-spline is well suited to interpolate sparse points by using a hierarchical structure at different refinement levels providing a C^2 continuous bicubic interpolation surface. A smooth surface for vertical correction was achieved with eight levels of iteration, providing a sufficient accuracy and avoiding the surface picking up of the finer details.

The final map of PSI velocities corrected by offset calibration (Fig. 11) is created by applying the v_{PSICorr} correction (Fig. 12, right) to the original PSI data set v_{PSIOrig}

$$v_{\mathrm{PSICal}} = v_{\mathrm{PSIOrig}} + v_{\mathrm{PSICorr}}. \quad (10)$$

E. Estimation of Errors

Total vertical errors are estimated as the square root of the squared sum of GNSS and SAR velocities and are shown in Fig. 13

$$\sigma_{\mathrm{GNSS+SAR}}^2 = \sigma_{\mathrm{GNSS}}^2 + \sigma_{\mathrm{SAR}}^2. \quad (11)$$

The two sources of errors in the interpolated GNSS data are those resulting from linear regression and those resulting from interpolation

$$\sigma_{\mathrm{GNSS}}^2 = \sigma_{\mathrm{regression}}^2 + \sigma_{\mathrm{interpolation}}^2. \quad (12)$$

Errors stemming from linear regression can easily be estimated as a by-product of regression analysis, as these errors mostly depend on the linearity of the time series, by checking for possible outliers and estimating annual and semiannual fluctuations. Errors associated with velocity measurements are estimated by modeling correlated noise with a combination of flicker and white noise.

These errors can be constrained only at the sparse locations of the GNSS sites. Errors associated with interpolation can also be estimated as a function that increases with distance from a known position and reaches its maximum at the most remote area. This method of error estimation is valid for each discrete point or pixel on the continuous GNSS velocity field.
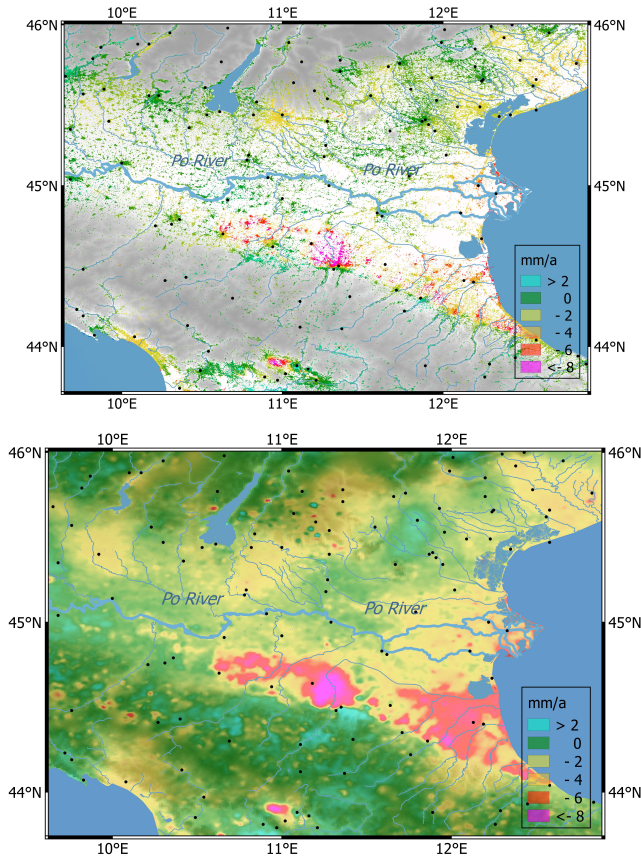
Fig. 11. Vertical velocities of (Top) sparse PSI points geodetically corrected by permanent GNSS stations and (Bottom) related continuous vertical velocity field derived by multilevel B-spline interpolation [31]. Green represents the stable area, cyan represents areas with uplift ≥ 2.0 mm/a, and yellow–orange–pink represents areas with subsidence ≤ -2.0 mm/a.

V. RESULTS AND DISCUSSION

The map of the vertical velocity field created by combining both the PSI and GNSS data sets and shown in Fig. 11 is extremely different from the map created with only SAR data (Fig. 6). The most important differences between these two maps are located along the Adriatic coast of Po Plain, which is characterized by a diffuse and constant subsidence from north to south.

In particular, by considering the vertical projection of the PS velocities after calibration and correction as visually reported in Fig. 12, the final map of Fig. 11 highlights a quite different situation with higher values of subsidence over the Adriatic coastal area compared to the previous map of Fig. 6. This is due to the GNSS calibration procedure that allows removing the effect of the low-frequency velocity component of interferometric data, mainly due to orbital errors. Therefore, a more realistic situation is provided, since the coastal area of Ravenna–Forlì cities, eastward of Bologna, is effectively affected by a wide historic ground lowering of about 6–7 mm/a located in correspondence of several rivers mouths and also extended up forward the inland [11]. This coastal area is thoroughly strongly weakened by marine erosion and human actions (i.e., urbanization, marine dunes demolition, and anthropic coastal infrastructure works) and the land subsidence is worsened due to
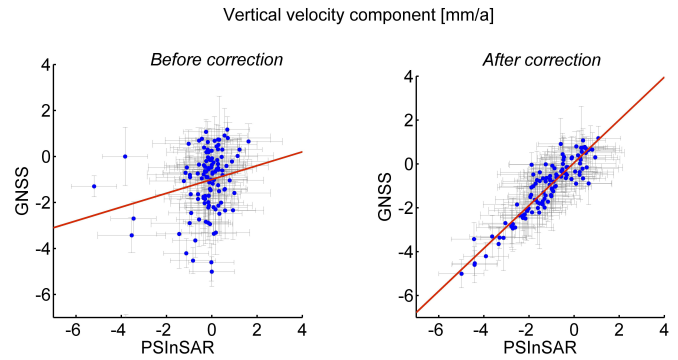

Fig. 12. Comparisons of GNSS and SAR vertical velocities calculated for each GNSS site (Left) before and (Right) after the corrections. SAR velocities are calculated by applying inverse distance weighting [37], [38] to a cloud of points approximately 100 m from each GNSS site. Orange lines represent the Pearson correlation between the two techniques. The coefficient of Pearson correlation is 0.34 and became 0.95 after the correction. The correlation coefficient of two random variables is a measure of their linear dependence. The Pearson correlation coefficient is defined as $\rho(A, B) = (\text{cov}(A, B)/\sigma_A \sigma_B)$, where σ_A and σ_B are the standard deviation of A and B, respectively.

underground fluids extraction and water over pumping from the aquifers.

More in detail, the area is characterized by minor subsidence along Po river plain with localized higher rates on the Po coastal delta along Adriatic Sea [13]–[17]. The highest ground lowering rates are recorded in the area spanning between Parma, Bologna, and Ravenna cities with maximum values higher than 8 mm/a N-NW of Bologna because of both natural and anthropogenic origins, due to presence of high thickness of plio–quaternary sediments and due to extensive groundwater withdrawals. These results are in line with works of Baldi *et al.* [15] and Carminati and Martinelli [16], stating the strongest subsidence areas were recorded in a zone north of Bologna, on the Po Delta, and on the coastal eastern area of Ravenna town.

Furthermore, the new map in Fig. 11 reveals that the north-western region of the Apennines is being slightly uplifted by about 2 mm/a. This outcome turns out to be in agreement with long-term displacement motion rates provided by geological data [41]–[43] and with results from [15] and [17] that assess that sites located in the northern part of the Apennine show uplift with a velocity ranging between 1.0 and 2.0 mm/a.

The adopted procedure for calibration can be useful also for analysis of SAR images acquired by different satellites, condition where single PS images cannot be combined due to their different acquisition characteristics (e.g., wavelength and orbit). Therefore, each SAR satellite mission produces a separate PS velocity surface, which is identified by the period of acquisition and by its own reference system. This situation will be the same for future missions, as the acquisition characteristics will be different. However, the creation of a single, unique surface motion map by merging different data sets is extremely important, in which geodesy plays an important role in the datum alignment of SAR products. The calibration method is necessary for calculating PSI velocities, as it is not possible to know *a priori* the velocities of the ground reference points used for stacking acquired SAR images. The knowledge of the relative motion between ground reference points of SAR images thus plays a fundamental role in
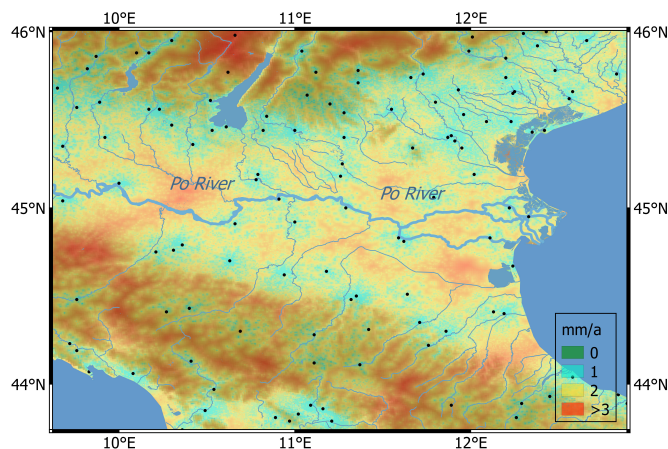
Fig. 13. Map of errors calculated by combining the error components of vertical velocity fields derived from PSI and GNSS permanent stations.

obtaining correct PSI velocities. The hypothesis that relative motion between ground reference points is constant can be assumed within a restricted area, but it will not hold for larger areas (i.e., on the regional, continental, or worldwide scales), and the GNSS geodetic velocity field must be applied to obtain correct results. For example, the Sentinel-1 PSI data set represents one of the possible applications of this method, as it was possible to expand the area of interest from a regional scale to a continental scale. Sentinel-1 regularly covers the globe, with a short revisit time of six days and the interferometric wide swath mode as its main acquisition mode over land. It acquires data with three subswaths using terrain observation with progressive scans SAR [44], producing 250 km of swath at a spatial resolution of 5 m by 20 m (single look).

As future outlook, the method of data analysis presented in this paper should be applied to validate PSI from newer SAR systems, such as Sentinel-1, COSMO-SkyMed SAR, and TerraSAR-X. The accuracy and density of the PS measurements obtained with these new SAR satellites make it possible to study fine-scale deformation phenomena that could not be detected by the old ERS and ENVISAT low-resolution SAR. In general, the theoretical condition to obtain correct results is to determine the velocities of reference points selected during SAR processing with GNSS observations, but most of time their positions are not provided with SAR products.

VI. CONCLUSION

PS SAR interferometry analysis represents a well-known and powerful technique used to detect and monitor surface movements of unstable areas at a detailed scale, such as unstable buildings and landslides, as well as wider-spread phenomena such as subsidence and uplift zones. GNSS represents the use of powerful instruments to realize a global reference system and to collect geodynamic data.

Combining these techniques (GNSS and SAR) produces a new technique that improves researchers' knowledge of surface movements for the following reasons.

Maps of surface movements that present correct information about velocities at both a detailed and a wider scale can be created, which improves current knowledge about processes involved in phenomena such as subsidence and uplift.

Geodynamics can be improved by SAR data that verify the stability of GNSS sites. It can also highlight the possible local movements that necessitate the use of a GNSS velocity site for geodetic purposes (i.e., crustal dynamics and reference frame).

SAR interferometry maps can be corrected for constant movements and for low wavenumber components of the velocity field before being aligned to geodetic data.

Because the different systems of acquisition of the SAR satellite mission produce velocity surfaces with different characteristics, it is necessary to create a unique surface motion map. Geodesy plays a fundamental role in the alignment of data before the stacking of the SAR maps.

REFERENCES

[1] D. P. S. Bekaert, P. Segall, T. J. Wright, and A. J. Hooper, "A network inversion filter combining GNSS and InSAR for tectonic slip modeling," *J. Geophys. Res. Solid Earth*, vol. 121, no. 3, pp. 2069–2086, 2016, doi: 10.1002/2015JB012638.

[2] M. Komac, R. Holley, P. Mahapatra, H. van der Marel, and M. Bavec, "Coupling of GPS/GNSS and radar interferometric data for a 3D surface displacement monitoring of landslides," *Landslides*, vol. 12, no. 2, pp. 241–257, 2015.

[3] E. Simonetto, S. Durand, J. Burdack, L. Polidori, L. Morel, and J. Nicolas-Duroy, "Combination of INSAR and GNSS measurements for ground displacement monitoring," *Procedia Technol.*, vol. 16, pp. 192–198, Jan. 2014.

[4] J. Catalão, G. Nico, R. Hanssen, and C. Catita, "Merging GPS and atmospherically corrected InSAR data to map 3-D terrain displacement velocity," *IEEE Trans. Geosci. Remote Sens.*, vol. 49, no. 6, pp. 2354–2360, Jun. 2011.

[5] A. Ferretti, C. Prati, and F. Rocca, "Permanent scatterers in SAR interferometry," *IEEE Trans. Geosci. Remote Sens.*, vol. 39, no. 1, pp. 8–20, Jan. 2001.

[6] M. Crosetto, O. Monserrat, M. Cuevas-González, N. Devanthéry, and B. Crippa, "Persistent scatterer interferometry: A review," *ISPRS J. Photogramm. Remote Sens.*, vol. 115, pp. 78–89, May 2016.

[7] P. A. Di, G. Nico, A. Pitullo, and G. Prezioso, "Monitoring Strategies of Earth dams by ground-based radar interferometry: How to extract useful information for seismic risk assessment," *Sensors*, vol. 18, no. 1, p. 244, 2018, doi: 10.3390/s18010244.

[8] F. Di Traglia *et al.*, "Tracking morphological changes and slope instability using spaceborne and ground-based SAR data," *Geomorphology*, vol. 300, pp. 95–112, Jan. 2018.

[9] C. Colesanti, A. Ferretti, C. Prati, and F. Rocca, "Monitoring landslides and tectonic motions with the permanent scatterers technique," *Eng. Geol.*, vol. 68, pp. 3–14, Feb. 2003.

[10] C. Doglioni, "Some remarks on the origin of foredeeps," *Tectonophysics*, vol. 228, pp. 1–20, Dec. 1993.

[11] L. Tosi, P. Teatini, T. Strozzi, L. Carbognin, G. Brancolini, and F. Rizzetto, "Ground surface dynamics in the northern Adriatic coastland over the last two decades," *Rendiconti Lincei*, vol. 21, pp. S115–S129, Dec. 2010.

[12] L. Tosi, P. Teatini, and T. Strozzi, "Natural versus anthropogenic subsidence of Venice," *Sci. Rep.*, vol. 3, Sep. 2013, Art. no. 2710, doi: 10.1038/srep02710.

[13] P. Teatini *et al.*, "Land subsidence due to groundwater withdrawal in the emilia-romagna coastland, Italy," in *Proc. 7th Int. Symp. Land Subsidence*, vol. 1, 2005, pp. 1–12.

[14] P. Teatini, L. Tosi, and T. Strozzi, "Quantitative evidence that compaction of Holocene sediments drives the present land subsidence of the Po Delta, Italy," *J. Geophys. Res., Solid Earth*, vol. 116, no. B8, p. B08407, 2011.

[15] P. Baldi, G. Casula, N. Cenni, F. Loddo, and A. Pesci, "GPS-based monitoring of land subsidence in the Po Plain (Northern Italy)," *Earth Planet. Sci. Lett.*, vol. 288, pp. 204–212, Oct. 2009.

[16] E. Carminati and G. Martinelli, "Subsidence rates in the Po Plain, northern Italy: The relative impact of natural and anthropogenic causation," *Eng. Geol.*, vol. 66, pp. 241–255, Nov. 2002.

[17] G. Bitelli, F. Bonsignore, and M. Unguendoli, "Levelling and GPS networks to monitor ground subsidence in the Southern Po Valley," *J. Geodyn.*, vol. 30, pp. 355–369, Feb. 2000.

[18] *IERS Conventions 2010*. Accessed: Nov. 20, 2011. [Online]. Available: www.iers.org

[19] *EUREF Guideline 2013*. Accessed: Nov. 20, 2017. [Online]. Available: www.epncb.oma.be

[20] J. Böhm, R. Heinkelmann, and H. Schuh, "Short note: A global model of pressure and temperature for geodetic applications," *J. Geodesy*, vol. 81, no. 10, pp. 679–683, 2007, doi: 10.1007/s00190-007-0135-3.

[21] L. Baroni, F. Cauli, G. Farolfi, and R. Maseroli, "'Final results of the Italian 'Rete Dinamica Nazionale' (RDN) of Instituto Geografico Militare Italiano (IGMI) and its alignment to ETRF2000," *Bull. Geodesy Geomatics*, vol. 68, no. 3, pp. 287–320, 2009.

[22] G. Farolfi and C. Del Ventisette, "Contemporary crustal velocity field in Alpine Mediterranean area of Italy from new geodetic data," *GPS Solutions*, vol. 20, no. 4, pp. 715–722, 2016, doi: 10.1007/s10291-015-0481-1.

[23] G. Farolfi and C. Del Ventisette, "Strain rates in the Alpine Mediterranean region: Insights from advanced techniques of data processing," *GPS Solutions*, vol. 21, no. 3, pp. 1027–1036, 2017, doi: 10.1007/s10291-016-0588-z.

[24] R. Dach, U. Hugentobler, P. Fridez, and M. Meindl, "Bernese GPS software version 5.0," Astronomical Inst., Univ. Bern, Bern, Switzerland, Tech. Rep. 640, 2007, p. 114.

[25] S. D. P. Williams, "CATS: GPS coordinate time series analysis software," *GPS Solutions*, vol. 122, pp. 147–153, Mar. 2008, doi: 10.1007/s10291-007-0086-4.

[26] M. Palano, "On the present-day crustal stress, strain-rate fields and mantle anisotropy pattern of Italy," *Geophys. J. Int.*, vol. 200, no. 2, pp. 969–985, 2014.

[27] T. A. Herring, R. W. King, and S. C. McClusky, "Introduction to GAMIT/GLOBK, release 10.4," Dept. Earth, Atmos., Planet. Sci., Massachusetts Inst. Technol., Cambridge, MA, USA, Tech. Rep., 2010, pp. 1–48.

[28] T. Herring, "MATLAB tools for viewing GPS velocities and time series," *GPS Solutions*, vol. 7, no. 3, pp. 194–199, 2003, doi: 10.1007/s10291-003-0068-0.

[29] Z. Altamimi, L. Métivier, and X. Collilieux, "ITRF2008 plate motion model," *J. Geophys. Res.*, vol. 117, p. B07402, Jul. 2012, doi: 10.1029/2011JB008930.

[30] C. Amante and E. W. Eakins, "ETOPO1 1 arc-minute global relief model: Procedures, data sources and analysis," Nat. Geophys. Data Center, Boulder, CO, USA, NOAA Tech. Memorandum NESDIS NGDC-24, 2009, p. 19. [Online]. Available: www.ngdc.noaa.gov/mgg/global/global.html.

[31] S. Lee, G. Wolberg, and S. Y. Shin, "Scattered data interpolation with multilevel B-splines," *IEEE Trans. Vis. Comput. Graphics*, vol. 3, no. 3, pp. 228–244, Jul. 1997.

[32] *Italian Geoportale Nazionale*. Accessed: Apr. 20, 2017. [Online]. Available: www.pcn.minambiente.it

[33] L. Solari, A. Ciampalini, F. Raspini, S. Bianchini, and S. Moretti, "PSInSAR analysis in the Pisa Urban Area (Italy): A case study of subsidence related to stratigraphical factors and urbanization," *Remote Sens.*, vol. 82, no. 2, p. 120, 2016.

[34] S. Bianchini and S. Moretti, "Analysis of recent ground subsidence in the Sibari plain (Italy) by means of satellite SAR interferometry-based methods," *Int. J. Remote Sens.*, vol. 36, no. 18, pp. 4550–4569, 2015.

[35] F. Cigna, S. Bianchini, and N. Casagli, "How to assess landslide activity and intensity with Persistent Scatterer Interferometry (PSI): The PSI-based matrix approach," *Landslides*, vol. 10, no. 3, pp. 267–283, 2013.

[36] G. Righini, V. Pancioli, and N. Casagli, "Updating landslide inventory maps using Persistent Scatterer Interferometry (PSI)," *Int. J. Remote Sens.*, vol. 33, no. 7, pp. 2068–2096, 2012.

[37] D. Shepard, "A two-dimensional interpolation function for irregularly-spaced data," in *Proc. ACM Nat. Conf.*, 1968, pp. 517–524, doi: 10.1145/800186.810616.

[38] P. M. Bartier and C. P. Keller, "Multivariate interpolation to incorporate thematic surface data using inverse distance weighting (IDW)," *Comput. Geosci.*, vol. 22, no. 7, pp. 795–799, 1996, doi: 10.1016/0098-3004(96)00021-0.

[39] G. Herrera *et al.*, "Analysis of subsidence using TerraSAR-X data: Murcia case study," *Eng. Geol.*, vol. 116, pp. 284–295, Nov. 2010.

[40] A. Brambati, L. Carbognin, T. Quaia, P. Teatini, and L. Tosi, "The Lagoon of Venice: Geological setting, evolution and land subsidence," *Episodes*, vol. 26, no. 3, pp. 264–268, 2003.

[41] U. Wegmüller, T. Strozzi, and C. Werner, "Land subsidence in the Po River Valley, Italy," in *Proc. Int. Geosci. Remote Sens. Symp. (IGARSS)*, Seattle, WA, USA, vol. 3, Jul. 1998, pp. 1376–1378.

[42] A. Argnani *et al.*, "Gravity tectonics driven by Quaternary uplift in the Northern Apennines: Insights from the La Spezia-Reggio Emilia geotransect," *Quaternary Int.*, vols. 101–102, pp. 13–26, Jan. 2003.

[43] V. Picotti and F. J. Pazzaglia, "A new active tectonic model for the construction of the Northern Apennines mountain front near Bologna (Italy)," *J. Geophys. Res., Solid Earth*, vol. 113, p. B08412, Aug. 2008, doi: 10.1029/2007JB005307.

[44] F. de Zan and A. M. Guarnieri, "TOPSAR: Terrain observation by progressive scans," *IEEE Trans. Geosci. Remote Sens.*, vol. 44, no. 9, pp. 2352–2360, Sep. 2006, doi: 10.1109/TGRS.2006.873853J.

Gregorio Farolfi received the master's degree in physics from the University of Bologna, Bologna, Italy, and the Ph.D. degree in earth sciences from the University of Florence, Florence, Italy.

He is currently an IT Coordinator with the Italian Geographic Institute, Florence, Italy. He was involved in oceanographic surveys. He has also a worldwide artistic activity. His research interests include geomatics, geodesy, satellite remote sensing, artificial intelligence, mathematical modeling, digital image fusion of multispectral, radar and positioning satellite data to study changes in the environment.

Silvia Bianchini received the degree in geology and the Ph.D. degree in earth science (engineering geology) from the University of Florence, Florence, Italy.

She is currently a Post-Doctoral Researcher with the Earth Sciences Department, University of Florence, and the Centre of Competence for hydro-geological hazards of the National Department of Civil Protection of the Italian Government. Her research interests include landslides mapping and monitoring, using radar spaceborne, airborne, and ground-based SAR data, and optical data.

Nicola Casagli is currently a Full Professor of engineering geology with the Earth Sciences Department, University of Florence, Florence, Italy. He is responsible for the Centre of Competence for hydro-geological hazards of the National Department of Civil Protection of the Italian Government. His research interests include geological hazards and ground instability, monitoring technology, engineering geological characterization and modeling.

Prof. Casagli is a Member of the National Committee for the Forecast and Prevention of Major Risks of the Department of Civil Protection of the Italian Government. He is a Vice President of the International Consortium on Landslides and a Vice President International Consortium on Geo-Disaster Reduction.